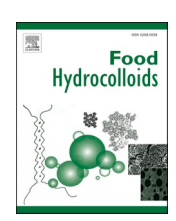


Contents lists available at ScienceDirect

### Food Hydrocolloids

journal homepage: www.elsevier.com/locate/foodhyd





# Improvement of lactoferrin thermal stability by complex coacervation using soy soluble polysaccharides

Tiantian Lin<sup>a</sup>, Younas Dadmohammadi<sup>a</sup>, Seyed Mohammad Davachi<sup>a</sup>, Hooman Torabi<sup>a</sup>, Peilong Li<sup>a</sup>, Benjamin Pomon<sup>a</sup>, Gopinathan Meletharayil<sup>b</sup>, Rohit Kapoor<sup>b</sup>, Alireza Abbaspourrad<sup>a,\*</sup>

<sup>a</sup> Department of Food Science, College of Agriculture and Life Sciences, Cornell University, Ithaca, NY, USA

#### ARTICLE INFO

Keywords: Lactoferrin Soy soluble polysaccharides Coacervates Electrostatic interaction Thermal stability Antimicrobial capacity OCM-D

#### ABSTRACT

Lactoferrin (LF) is a multifunctional protein in the transferrin family that has been widely used in food and pharmaceutical products. However, it is susceptible to denaturation during thermal processing, which can diminish the functionality and bioavailability of LF in the final product. Coacervation of LF with biopolymers has been demonstrated as a promising approach to protect LF from thermal denaturation. This work aims to study the formation conditions, structural characteristics, and interaction mechanisms of soy soluble polysaccharides (SSP) and lactoferrin coacervate complex (SSP-LF), and to investigate the effect of the SSP-LF complex on the structural changes and antimicrobial capacity of LF before and after thermal treatment. Either soluble and insoluble SSP-LF complexes could be formed depending on the pH (4–7) and ratios (SSP: LF = 8:1 to 1:16), according to the turbidity, zeta-potential, and particle size analysis. Electrophoresis, SEM, FTIR, and CD spectra measurement suggested that the SSP-LF complex could maintain the secondary structures of LF. Quartz crystal microbalance with dissipation (QCM-D) was used to elucidate the real-time interactions between SSP and LF, showing that the major driving force to form complexes was electrostatic interaction. The SSP-LF complex was able to prevent the aggregation/denaturation of LF and the loss of the  $\alpha$ -helix during thermal treatment at neutral pH. The SSP-LF complex maintained the antimicrobial capacity of LF after thermal treatment. The improved thermal stability and functionality of the SSP-LF complex could facilitate the application of LF in various commercial products.

#### 1. Introduction

Lactoferrin (LF), also known as lactotransferrin, is a multifunctional protein in the transferrin family. It is present in many biological fluids such as milk, saliva, and seminal fluid (Lönnerdal & Iyer, 1995). LF is a single polypeptide globular glycoprotein with a molecular weight of around 80 kDa (Lönnerdal & Iyer, 1995; Moore et al., 1997). The tertiary structure of LF is made of two homologous lobes (N- and C-lobes), connected through a short  $\alpha$ -helix. Each lobe can be divided into two similar sized sub-domains: N1&2 and C1&2 (Wang et al., 2019). Biological functions of LF include the binding and transport of iron and the promotion of iron absorption in the body. It promotes cell growth and detoxifies harmful free radicals and has anti-bacterial, anti-viral, anti-inflammatory, and anti-carcinogenic properties (King et al., 2007; Lönnerdal & Iyer, 1995; Vogel, 2012). Currently, the capacity of LF to

inhibit the growth of microorganisms including bacteria and viruses is of increasing interest for example, LF inhibits a wide range of foodborne pathogens (Conesa et al., 2010; Jenssen & Hancock, 2009). Emerging studies have indicated that LF has potential therapeutic function for the prevention of COVID-19 as it helps to inhibit the SARS-CoV-2 virus infection in various in vitro cell models(Campione et al., 2021; Mirabelli et al., 2021; Wotring et al., 2022). Thus, adding LF to food ingredients has significant potential for assisting and bolstering the human immune system.

However, LF is sensitive to denaturation induced by thermal processing, which causes structural changes and the loss of biological functionality (Bokkhim et al., 2015; Brisson et al., 2007). Therefore, strategies are needed to minimize the undesired thermal denaturation of LF during the processing of LF-containing products. According to the iron saturation level, where two Fe $^{+3}$  ions covalently bound to an LF

<sup>&</sup>lt;sup>b</sup> National Dairy Council, Rosemont, IL, USA

<sup>\*</sup> Corresponding author. Department of Food Science, College of Agriculture and Life Sciences, Cornell University, Ithaca, 14853, NY, USA. *E-mail address:* alireza@cornell.edu (A. Abbaspourrad).

molecule is considered 100% saturation, LF is classified as apo-LF (<15% of iron), natural-LF (15-20% of iron), and holo-LF (>20% of iron). Apo-LF denatures at ~70 °C, whereas holo-LF denatures at ~90 °C, and natural-LF denatures between 70 °C and 90 °C (Bokkhim et al., 2013). This trend suggests that increasing the iron saturation of LF could be a strategy to reduce the thermal denaturation of LF, however, it is still not adequately effective in protecting LF during commercial pasteurization conditions which is usually higher than 75 °C (Wang et al., 2019). PEGylation and microencapsulation via liposomes or bilayers, respectively, have also been used to protect LF against harsh gastric environments (Kilic et al., 2017; Nojima et al., 2008; Yao et al., 2015). Unfortunately, these methods usually involve complicated formulation procedures and the usage of synthetic chemicals, which make them either impractical or economically unfeasible in the food industry (Lin et al., 2021). Alternatively, the complex coacervation of LF with polysaccharides or proteins is recognized as a promising approach to protect LF from thermal denaturation. Specifically, the simple development processes and easy-to-scale-up features are its major

The complex coacervation process involves at least two oppositely charged biopolymers in an aqueous medium that forms a coacervate complex at a specific pH, ionic strength, and biopolymer mixing ratios (de Kruif et al., 2004). LF is positively charged over a large pH range (<8) and is soluble in water at any pH except for the isoelectric point that occurs between 8 and 9 (Bokkhim et al., 2013). These features facilitate the formation of complex coacervation of LF with many anionic bio-compounds. Many studies have been conducted to investigate the formation of complex coacervates of LF with polysaccharides including gum arabic (da S. Gulão et al., 2014), pectin (Bengoechea et al., 2011), and sodium alginate (Bastos et al., 2018; Wang, Blanch, et al., 2017), etc. However, very few of them examined whether, or how, the formed coacervate complex improved the thermal stability of lactoferrin and much less of them have tested if the formed complex could maintain the functionality, such as antibacterial capacity, of lactoferrin after thermal processing.

As byproducts obtained downstream from the food industry, soy soluble polysaccharides (SSP) have demonstrated potential use as sustainable and low-cost biopolymers to form a coacervate complex with LF. The structure of SSP has been extensively studied and is wellunderstood. The main backbone of SSP consists of rhamnogalacturonan and homogalacturonan chains, branched by arabinose and galactose, and contains 18% galacturonic acid (Nakamura et al., 2001). The negative charge of SPP mainly comes from carboxylate groups, and its pKa is around 2 to 3. It has been reported that the high content of side-chains and natural sugars make SPP more soluble and prevent aggregation of the proteins (Nakamura et al., 2004). A recent study also demonstrated that SSP showed a superior ability to maintain the colloidal stability of whey protein than pectin (Zamani et al., 2020). Another study showed that the iron-LF complex and its mixture with SSP showed an improved thermal stability than native LF, however whether SSP itself can improve the thermal stability of LF was not investigated (Ueno et al., 2012). To date, no study has been reported on the formation of SSP-LF coacervate complex and the examination of its thermal stability. To better understand these, it is necessary to elucidate the interactions of SSP and LF during the formation of complex coacervates and their effect on the thermal stability and functional properties of LF.

To this end, the overall goal of this work is to develop a feasible, and technically simple approach using complex coacervation of LF with SSP to improve the structural and functional stability of LF to thermal treatments, particularly in regard to its antibacterial capacity. The specific objectives of our study were to: 1) investigate the conditions for the complex coacervation of LF with SSP and study the morphology and structure of the formed complex; 2) confirm the interaction level between LF and SSP using a quartz crystal microbalance with dissipation (QCM-D); 3) evaluate the effect of the formed complex on the thermal stability, structural conformation, and antibacterial properties of LF.

The results obtained from this work could potentially enable the food industry to formulate LF based ingredients with enhanced thermal stability and functionality and further use it in powdered formulas or ready to drink products.

#### 2. Materials and methods

#### 2.1. Materials

The LF powder (natural bovine LF, Bioferrin 2000; Iron >15 mg/100g) was provided by Glanbia Nationals, Inc, Fitchburg, WI). Soy soluble polysaccharides (SSP) were provided by Fuji Oil (Japan). The reagents for electrophoresis were purchased from Bio-Rad Laboratories (Hercules, CA, USA). The 1-hexadecanethiol (purity >97.0%) was purchased from TCI Chemicals (Tokyo Chemical Industry, Tokyo, Japan). Hydrochloric acid, sodium hydroxide, ammonia, hydrogen peroxide, and ethanol (200 Proof) were purchased from Fisher Scientific (Hampton, NH, USA). Luria broth (LB), LB agar were purchased from Sigma-Aldrich (St. Louis, MO, USA). Milli-Q water (18.2  $\mathrm{M}\Omega/\mathrm{cm})$  was prepared from a Millipore water purification system (Millipore Sigma, Burlington, MA, USA).

#### 2.2. Preparation of SSP-LF complex coacervate

Stock solutions of LF (5%, w/v) and SSP (2%, w/v) were prepared by dissolving LF or SSP into Milli-Q water and mixed for 2 h at room temperature (25 °C). Both stock solutions were allowed to settle overnight at 4 °C. Working solutions (1%, w/v) were then prepared by diluting stock solutions with Mili-Q water. Three common methods were used to prepare the SSP-LF complex: pH-first, pH-low-to-high, and pH-high-to-low method. For the pH-first method, working solutions were adjusted to the target pH (4, 5, 6, and 7) first using 1 M or 0.1 M NaOH or HCl. LF and SSP solutions were mixed at different ratios, keeping the total biopolymer concentration to 1% w/v. The pH of the mixture was reconfirmed within the target pH range of  $\pm$ 0.25. The mixture was stirred for 30 min before measuring the turbidity, particle size, and zeta-potential of mixture solutions.

For the *pH-low-to-high* method, LF and SSP working solutions (1%, w/v) were mixed at pH 2.5 in different ratios and then the solution mixture was gradually adjusted to the target pH by adding sodium hydroxide (0.1 M) with constant magnetic stirring. For the *pH-high-to-low* method, LF and SSP solutions were mixed at pH 10.25 in different ratios and then the solution mixture was gradually adjusted to the target pH by adding hydrochloric acid (0.1 M) with constant magnetic stirring. All experiments were performed at room temperature (25  $^{\circ}$ C).

The SSP-LF coacervate complex was collected by centrifuging the SSP-LF mixtures (prepared from *pH-first* method) at 20,000g and 4 °C for 30 min. The collected pellets were frozen (-20 °C) overnight and then freeze dried (Labcono, Kansas, MO, USA) for 36–48 h, at a vacuum pressure of -0.175 mBar and moisture collector temperature of -53 °C.

#### 2.3. Thermal treatment of LF and SSP-LF mixtures

Samples including LF, SSP-LF mixtures, and rehydrated SSP-LF complex solutions were loaded into glass tubes and placed into a water bath at different temperatures (75  $^{\circ}$ C, 85  $^{\circ}$ C, and 95  $^{\circ}$ C) for 2 min (it took approximately 100 s to reach equilibrium and it was held at the target temperature for approximately 15–20 s) and then immersed in an ice-water bath to cool down to ambient temperature (25  $^{\circ}$ C) before further analysis.

#### 2.4. Characterization

#### 2.4.1. Turbidity measurements

The turbidity of the LF and SSP-LF mixtures were measured using a UV-Vis light spectrophotometer (UV-2600, SHIMADZU Co., Japan). The

transmittance was measured at 600 nm using 1 cm path-length quartz cuvettes at room temperature (Zheng et al., 2020). Milli-Q water was used as the blank (100% transmittance). The turbidity (T) was calculated according to the following equation (Eq. (1)):

$$T = -\ln\frac{I}{I_0} \tag{1}$$

where I is the transmittance intensity of samples and  $I_0$  is the transmittance intensity of the blank.

#### 2.4.2. Particle size measurements

The average diameter and particle size distribution of LF, SSP, and SSP-LF mixtures were analyzed using the dynamic light scattering instrument (Zetasizer Nano-ZS, Malvern, Germany). All analyses were performed at 25  $^{\circ}\text{C}$  in a 1-cm path-length cuvette at the wavelength of 633 nm and a backscattering angle of 173  $^{\circ}$ . The refractive index of dispersant was set as 1.330 and the refractive index of material was set as 1.45. Analysis was done in triplicate with at least 11 runs for each measurement.

#### 2.4.3. Zeta-potential measurements

The zeta-potential of LF, SSP, and SSP-LF mixtures were measured using the Nano-ZS (Malvern, Germany) using Smouluchwski mode. The software could determine the suitable type of measurements after obtaining the sample conductivity using the voltage of about 150 V. Samples were measured in triplicate with 10 runs for each measurement.

#### 2.4.4. Circular dichroism (CD) spectroscopy analysis

The secondary structures of lactoferrin after complex formation and heat treatment were measured using CD spectroscopy. The CD spectra of LF, SSP, and SSP-LF mixtures were measured using an AVIV-202-01 spectropolarimeter (Lakewood, NJ, USA) in the far-UV region (190–260 nm) at 25 °C. To reduce the gain, samples were diluted to 0.02% LF before measurement. Samples were analyzed in a quartz cell with a 1-mm path length. The obtained data were converted to molar ellipticity, [ $\theta$ ] (deg cm<sup>2</sup> dmol<sup>-1</sup>), using the DichroWeb online processing platform (Z. Zhang et al., 2021).

#### 2.4.5. Differential scanning calorimetry (DSC) analysis

The thermal properties of the LF and SSP-LF coacervate complex were analyzed through a differential scanning calorimeter (DSC, Q200, TA Instruments, New Castle, DE, USA). The freeze-dried proteins and complex powder (~3 mg) were measured in a standard aluminum pan. Ten microliters of Milli-Q water were added to pre-hydrate samples for at least 2 h after being sealed. An empty sealed aluminum pan was used as a reference. The samples were further equilibrated for 10 min in the sample analysis chamber before starting the heating scanning cycle from 25 °C to 110 °C at 5 °C/min. The onset temperature ( $T_0$ ), peak temperature ( $T_p$ ), conclusion temperature ( $T_c$ ), and enthalpy change ( $\Delta$  H) of the thermal transitions were analyzed using the Universal Analysis 2000 software (TA instruments).

#### 2.4.6. Fourier transform infrared spectroscopy (FTIR) analysis

The FTIR spectra of freeze-dried LF, SSP, and SPP-LF complex were performed to analyze using an IRAffinity-1S Spectrometer with a single-reflection attenuated total reflectance (ATR) accessory from the Shimadzu Corporation (Kyoto, Japan). FTIR was analyzed to assess any changes in chemical bonds in both biopolymers after forming co-acervates. The measurement was performed in an average of 32 scans from 500 to 4000 cm<sup>-1</sup> at a resolution of 4 cm<sup>-1</sup>. A background was tested before sample analysis under the same testing conditions.

#### 2.4.7. Microstructure analysis

The microstructure of LF and SSP-LF samples was observed using the Field-emission scanning electron microscope (SEM) (Zeiss Gemini 500,

Jena, Germany). Both freeze dried samples and solution samples were analyzed. An aliquot ( $\sim\!10~\mu L)$  of the solution was dropped on the pin stub with carbon tape and then vacuum dried overnight in the desiccator. Samples were coated with Au/Pd in a sputter coater (Denton Desk V, NJ, USA) before being scanned and photographed by a high efficiency secondary electron detector with a 20.0  $\mu m$  aperture. The accelerating voltage was 1 kV.

#### 2.4.8. Electrophoresis analysis

LF in the mixture solutions and supernatants after centrifugation was analyzed using sodium dodecyl sulfate (SDS)-PAGE in a vertical mini gel electrophoresis system (Mini-PRO-TEAN Tetra cell, Bio-Rad, USA). The premixed TGA fast Cast Acrylamide starter kit was used for the preparation of PAGE gels. Twenty microliters of diluted samples (2 mg/mL of protein) were mixed with 2X Laemmli buffer at the ratio of 1:1 and then heated in a boiling water bath for 5 min. Then 20  $\mu$  L of mixtures were loaded on the gels for electrophoresis (200 V) for about 30–45 min. The gel was stained in 0.15% (w/v) Coomassie Brilliant R-250 solution which consisted of 50% (v/v) methanol and 10% (v/v) acetic acid for half an hour. Then the gel was de-stained in de-staining solutions (20% (v/v) methanol and 10% (v/v) acetic acid) for 24 h (Z. Zhang et al., 2021).

#### 2.4.9. Antimicrobial activity analysis

A strain of Staphylococcus aureus was used in this study as the target bacteria. This strain was isolated by the Animal Health Diagnostic Center of Cornell University (AHDC) from bovine feces. It was kept in Luria broth (LB) agar medium with 20% glycerol and stored at -70 °C. Both LB broth and agar medium were prepared and autoclaved at 121 °C for 15min. The Staphylococcus aureus were grown on LB agar medium for 24 h. A loop of a pure colony from the medium was transferred into a 10 mL fresh LB medium for 24 h of incubation at 37  $^{\circ}$ C. Then the culture was diluted 10 times with LB medium and mixed with unheated or heated LF-SSP solutions, LF or SSP solutions, or an equivalent volume of milli-Q water as a control. The culture with different samples was then diluted four-, five-, or sixfold through a series of dilutions in the PBS buffer following a previous study (Niu et al., 2019). The diluted culture (1 mL) was inoculated in LB agar plate medium and incubated for 24 h at 37 °C. The bacterial growth was observed at 24 h and an image was taken at 24 h to count the colony-forming units.

## 2.4.10. Real-time interaction analysis of lactoferrin and soy soluble polysaccharides

To further elucidate the electrostatic interactions between LF and SSP at molecular levels, the quartz crystal microbalance with dissipation (QCM-D) techniques were used. A QSense Analyzer system from Biolin Scientific (Gothenburg, Sweden) equipped with gold sensors (QSX 301, 4.95 MHz) was used. The gold sensor was first cleaned followed by the procedure according to (Yan et al., 2021). The gold sensor was then modified to provide a hydrophobic surface by immersing in 2 mM 1-hexadecanethiol in ethanol for at least 20 h at room temperature (Teo et al., 2016). The hydrophobic surface would enable protein absorption on the gold surface mainly driven by hydrophobic interactions, thus minimizing any influences on the interactions (mainly electrostatic interactions) between SSP and LF. The contact angle of the gold sensors with milli-Q water, before and after modification were 80° and 97° (Fig. S1), as determined by a contact angle goniometer (Rame-Hart 500 model, Rame-Hart Instrument, Co, Succasunna, NJ, USA). For the regeneration of the gold sensor, after each test, the gold sensors were cleaned and modified using the same cleaning and modification procedures.

LF and SSP solutions at 1% (w/v) in Milli-Q water were prepared at target pH 4, 5, 6, or 7. Each QCM-D experiment was pre-equilibrated with Milli-Q water (at the trial specified pH) to reach a baseline signal before injecting protein solution. The LF solutions were then injected into the system and flow over the sensor at a rate of  $0.1 \, \text{mL/min}$ . When

the signal became stable, it indicated an equilibrium was reached. Milli-Q water at the same pH was injected into the system to remove the weakly-adsorbed LF as an intermediate rinsing step. Then the SSP solution at the same pH was then injected into the system until equilibrium, followed by rinsing with Milli-Q water. The above steps were repeated at pH 4, 5, 6, and 7. The temperature and flow rate were kept consistent for each experiment.

For each QCM-D experiment, the changes of resonance frequency and dissipation were recorded at several overtones and then calculated as the mass adsorbed on each layer of molecules using the Broadfit model through the DFind software (QScense, Biolin Scientific, Gothenburg, Sweden).

#### 2.5. Data analysis

The obtained data were presented as means and standard deviations of duplicates or triplicates and analyzed using Analysis of Variance (ANOVA). The difference between mean values was evaluated using the Tukey HSD comparison test (P < 0.05). All the statistical analyses were performed using JMP Pro15 (SAS Institute, USA) and plotted by GraphPad Prism9 (GraphPad Software Inc., USA).

#### 3. Results and discussion

## 3.1. Effect of SSP:LF ratio and pH on the formation of coacervate complexes

The effect of pH and mass ratio on the formation of SSP-LF complexes was studied using the *pH-first* method. In this method, SSP and LF solutions (1%, w/v) were individually adjusted to pH 4, 5, 6, or 7, and then both biopolymers at the same pH were mixed at a series of mass ratios of SSP: LF from 8:1 to 1:12. Fig. 1 shows the turbidity and visual appearance of SSP-LF mixtures with different mass ratios at pH 4–7. Turbidity is one of the primary indicators showing the formation of insoluble/soluble complex coacervation. The mixture with the highest turbidity was generally indicated for the optimal conditions of complex coacervation. Generally, along with the increasing pH, a higher ratio of LF was required to obtain the highest turbidity (Fig. 1A–D), which was due to the change of charges of SPP and LF at each pH value (explanation is given in Fig. 2). For each pH, the ratio at which the highest turbidity was

found differed: at pH 4, the SSP:LF ratio of 1:2 provided the highest turbidity; at pH 5, the SSP:LF ratio of 1:4 provided the highest turbidity; at pH 6, the SSP:LF ratio of 1:8 provided the highest turbidity; and at pH 7, the SSP:LF ratio of 1:12 provided the highest turbidity. SSP-LF mixtures formed a large quantity of insoluble complexes at pH 4 and 5 at optimal ratios, while they formed a limited quantity of insoluble complexes or predominately soluble complexes at pH 6 and 7 at optimal ratios (Fig. 1). At all pH conditions, the SSP-LF mixtures exhibited the highest turbidity at pH 5, indicating the optimal conditions and highest yield for the complex coacervation.

To further understand the phenomena of the turbidity changes of SSP-LF mixtures at different mass ratios and pH, their charge and mean particle size were investigated and illustrated in Fig. 2. A-E and a-e, respectively. As shown in Fig. 2A, LF solutions have a positive charge (+2-20 my) from pH 4 to 7 while SSP have a negative charge (-7-13)my). According to other studies, the pI of LF is near 8.0, and the pKa of SSP is close to 3.5 (Wang et al., 2019; Zamani et al., 2020). Thus, the optimal pH for the formation of the SSP-LF electrostatic complex is in the range of pH 3.5 to 8.0 when two polymers pose opposite charges. When the two biopolymer solutions at pH 4 were mixed, the zeta-potential was negative at the SSP:LF ratios of 8:1, 4:1, 2:1, and 1:1, and was positive at the SSP:LF ratios of 1:4, 1:8. At the SSP:LF ratio of 1:2, charge balance is achieved, and better interactions for complex formation occurs. At pH 5, the ratio of SSP:LF that produced the net-zero charge of SSP:LF mixtures shifted from 1:2 to 1:4, requiring a higher ratio of LF to balance the charge of SSP. Similarly, with the increasing of pH to 6 and 7, the "optimal" ratios to achieve the charge balance of SSP:LF mixtures were shifted to 1:8 and 1:12 for pH 6 and pH 7, respectively. Similar to reported studies in protein-polysaccharides mixtures (Bastos et al., 2018; Bengoechea et al., 2011), these optimal ratios showing net-zero charges of SSP:LF mixtures were consistent with the ratios presenting the highest turbidity of the SSP:LF mixture (Fig. 1) at the corresponding pH conditions. This implies that the electrostatic interactions between SSP and LF were the major driving force for the complex coacervation of SSP and LF.

The mean particle size of SSP, LF, and the SSP-LF mixtures was also measured and shown in Fig. 2a-e. For individual SSP and LF solutions, the mean particle size diameter of LF was ranging from 30 to 60 nm, at all pH levels. Conversely, the mean particle size of SSP was between 300 and 400 nm at all pH levels (Fig. 2a). Because of the increased proportion of LF which is in smaller size than SSP, the mean size of SSP-LF

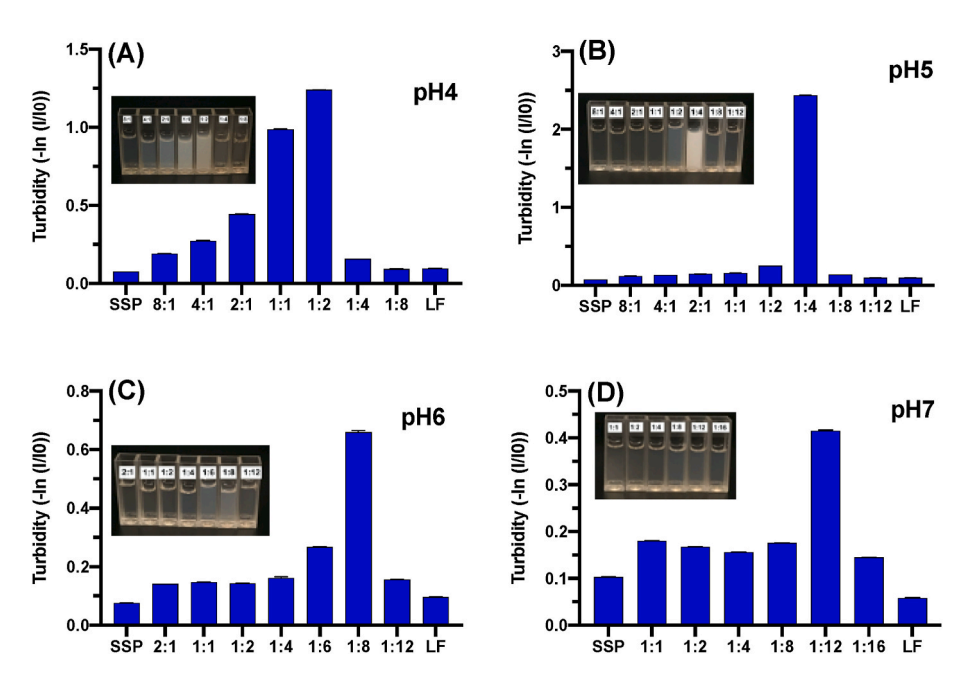


Fig. 1. Turbidity and optical images of SSP-LF mixtures at pH 4, 5, 6, and 7 (A-D), prepared by the pH-first method.

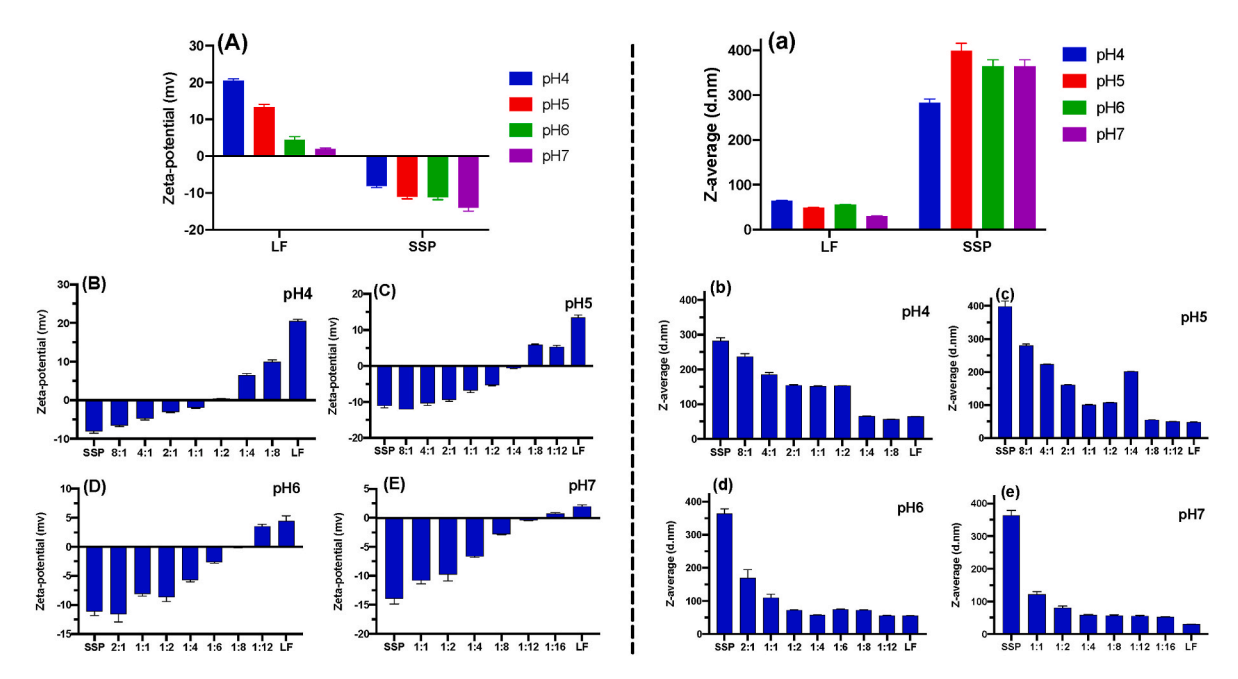


Fig. 2. Zeta-potential (A-E) and mean particle size (a-e) of LF, SSP and SSP-LF mixtures at pH 4, 5, 6, and 7, prepared by the pH-first method.

mixtures was expected to be gradually decreased when the ratio of SSP: LF was changed ranging from 8:1 to 1:16 (Fig. 2b-e). However, the formation of complex coacervation at the ratio of 1:1 and 1:2 at pH 4, as indicated by the increased turbidity, may increase the portion of the larger-sized complex, thus the mixtures did not show a decreased particle size (Fig. 1A). This phenomenon was more clearly illustrated at pH 5 (Fig. 2c) when the mean particle size was significantly increased at the ratio of 1:4 (~200 nm), due to the formation of complex coacervate, compared to the mixtures at the ratio of 1:1 and 1:2 ( $\sim$ 100 nm), even though the former mixture was prepared with a higher proportion of the relatively smaller LF particles. These results were consistent with the highest turbidity of LF at the ratio of 1:4 at pH 5 (Fig. 1B). Similarly, the mean particle size of mixtures at pH 6 and pH 7 was gradually decreased along with the increased proportion of LF, except for the conditions exhibiting the highest turbidity (1:8 at pH 6 and 1:12 at pH 7). At each optimal condition, the SSP-LF mixture showed a mean particle size of 100-250 nm at pH 4 and 5, while it was less than 100 nm at pH 6 and 7 due to weaker electrostatic interactions between SSP and LF at pH 6 and 7 and therefore less complex formation.

The PSD of LF, SSP, and SSP-LF complexes at various pH levels and ratios are shown in Fig. S2. The PSD of SSP showed one peak at 1-100 nm and another peak around 1000 nm. The PSD of SSP obtained in the current study was similar to previously reported studies (D.-Y. Zhang et al., 2021). Pure SSP solutions did not seem to be fully dispersed as a single molecule and tended to self-associate especially in acidic pH where SSP possessed a lower negative charge and as a result a decreased electrostatic repulsion. For the SSP-LF mixtures, initially, more than one peak was shown on the PSD graph as the solutions were simply a mixture of biopolymers. When the optimal ratios for complex formation was reached for each pH, the individual peaks coalesced into a single peak as the complex formed. For example, at pH 5, only the ratios of 1:4 and 1:8 showed one predominant peak while other ratios showed multiple peaks (Figs. S2-B). Due to the stronger electrostatic interactions between oppositely charged SSP and LF, when LF was mixed with SSP, the SSP polymers dissociated from each other and showed a preference to associate with LF. Particularly, at optimal complexation ratios and pH levels (SSP: LF = 1:2 at pH 4 and 1:4 at pH 5). At these conditions, the SSP-LF complex was predominately formed and only one peak was shown in PSD results at  $\sim$ 100–1000 nm. This also helps to explain why the mean size of SSP showed a higher value than the complex of SSP-LF

formed at the ratio of 1:4 to pH 5 (Fig. 2c). When the PSD of SSP solution and SSP-LF mixtures exhibited two separated peaks and therefore would not be considered monodispersed, the mean size may not reflect the actual size of particles. Overall, PSD results provided a complementary explanation with the mean particle size of the SSP-LF biopolymer solutions/complexes.

The pH-low-to-high and pH-high-to-low approaches were also investigated to find the pH-induced phase transitions on the formation of the SSP-LF complex. The effect of pH on the formation of SSP-LF complex during the titration by base and acid is illustrated in Fig. 3B–E and b-e, respectively. First, the turbidity of the individual SSP and LF solutions at 1% (w/v) was measured to distinguish the biopolymer self-aggregates from the formation of the complex coacervation. There was an increase of turbidity in LF solution when the pH was increased to pH 7 or higher. As the pH approached the pI of LF it caused self-aggregation of proteins, which was also be observed in the PSD of the LF solutions (Fig. S2). However, this turbidity increase was slight (from 0.05 to around 0.1), and both SSP and LF solutions showed low turbidity (<0.2) in all pH ranges.

In the pH-low-to-high method, solutions at the SSP:LF ratio of 1:2 showed a broad pH range (3.0-5.5) with a turbidity higher than 0.2 indicating the formation of coacervates. The highest turbidity at 0.65 occurred at around pH 4 and this pH value was called pHopt, to represent the optimal pH condition for the coacervate formation. When the solution was prepared at an SSP:LF ratio of 1:4, the titration process showed a typical phase diagram during the formation of coacervate (Fig. 3C). Four critical pH levels were identified:  $pH_c$ ;  $pH_{\omega 1}$ ;  $pH_{opt}$ ;  $pH_{\omega 2}$ .Initially, at low pH close to the pKa of SSP, the turbidity was very low and no complex formed. The pH<sub>c</sub> represents the pH when SSP and LF solutions started to form SSP-LF complexes. The complex that initially formed was small and soluble due to weak interactions between the biopolymers and the turbidity of solutions started to increase gradually. At  $pH_{\omega 1}$ , there was a sharp increase of turbidity, indicating the formation of an insoluble complex. As the pH increased, the solutions reached its highest turbidity at  $pH_{opt}$  the optimal pH for the formation of the SSP-LF coacervate complex. After  $pH_{opt}$ , the solution turbidity dropped sharply until there was no further observable decrease in turbidity. At this point, the pH was termed as  $pH_{\omega 2}$ , indicating the endpoint of complex formation. This typical phase transition diagram was also observed at the biopolymer solutions with SSP:LF ratio at 1:8 (Fig. 3D). The four critical

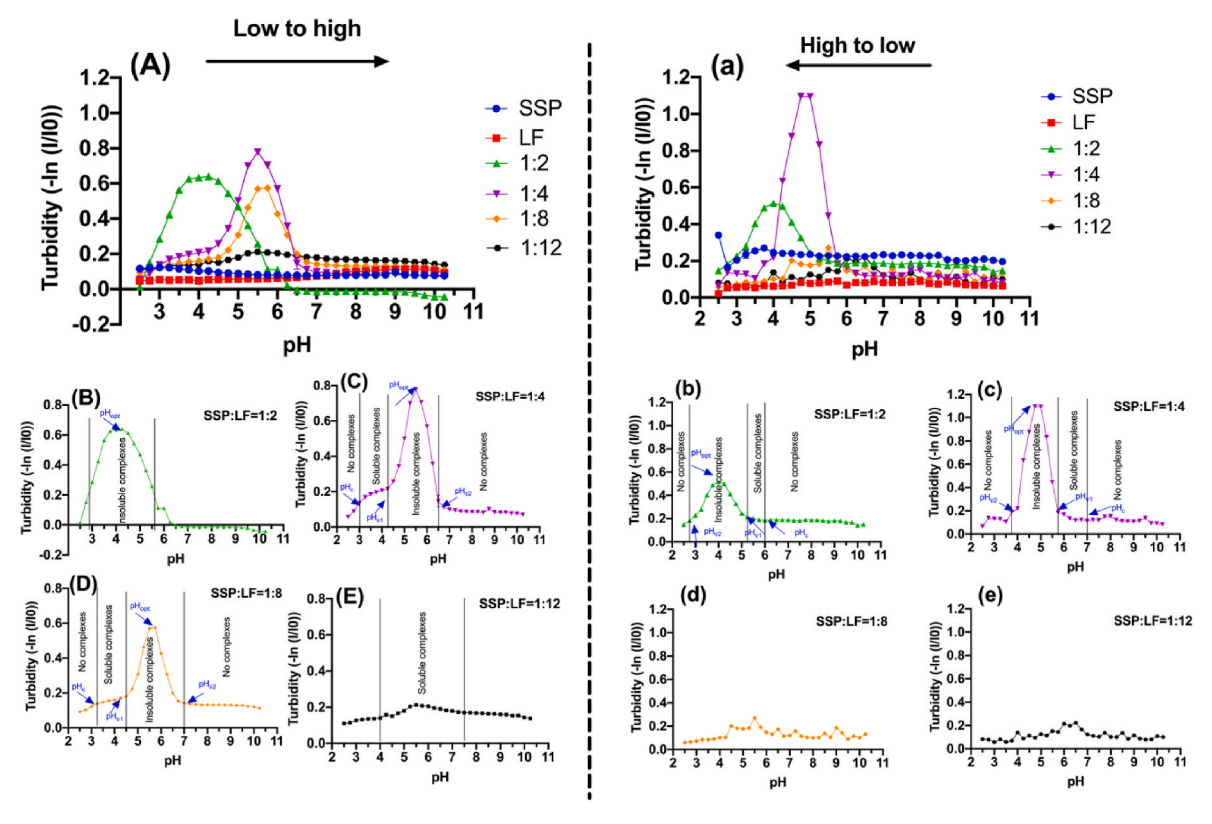


**Fig. 3.** Turbidity of SSP-LF mixtures prepared by the *pH-low-to-high* (A) and *pH-high-to-low* (a) method at various pH and SSP/LF mass ratios. Phase transitions diagrams of SSP-LF mixtures at SSP/LF mass ratios of 1:2, 1:4, 1:8 and 1:12 prepared through *pH-low-to-high* (B–E) and *pH-high-to-low* method (b–e).

pH levels were shifted towards the larger side of pH along with the increased ratio of LF in SSP/LF solutions. This shift is indicative that less positive charges from LF (closer to pI) and more negative charges from SSP (away from pKa) were needed to neutralize the zeta potential and form complexes. A similar phase transition trend was also reported in solutions consisting of LF and other oppositely charged biopolymers such as soy protein isolates (Zheng et al., 2020) and gum Arabic (da S. Gulão et al., 2014). At the ratio of 1:12, the turbidity was quite low, thus only soluble complexes were formed (Fig. 3E). This was consistent with the result obtained from the pH-first method at similar ratios, in which no significant increase of turbidity was observed.

For the pH-high-to-low method, interestingly, only the SSP/LF ratios of 1:2 (Figs. 3b) and 1:4 (Fig. 3c) were able to form coacervates and demonstrated the typical phase transition diagram. Both the ratios 1:8 (Figs. 3d) and 1:12 (Fig. 3e) did not generate any increase in turbidity (from 0 to 0.2) during the titration process. These results mean that titration direction does impact the formation of coacervates. Titration direction can also change the pH at which we find a soluble complex, which is always formed just before the insoluble complex evidenced by the slight rise in turbidity. Specifically, at the pH-low-to high-method,  $pH_{\varphi 1}$  was on the left side of  $pH_{opt}$  while at the *pH-high-to-low* method,  $pH_{\varphi 1}$  was on the right side of  $pH_{opt}$ . Lastly, among all the solutions prepared by both methods, the highest turbidity was observed at ratio 1 to 4 with pH<sub>opt</sub> around pH 5 using the pH-high-to-low method, indicating the highest yield of coacervate as well. However, the highest turbidity obtained using the pH-first method was higher than the one obtained using the pH titration methods. Generally, although the pHopt and turbidity values were influenced by these three methods, the trends were similar, so all the complex samples after this section were prepared using the pH-first method.

The effect of ionic strength (0-500 mM) on the SSP-LF coacervate formation was also preliminarily tested on the SSP-LF complex at optimal pH levels and ratios (Fig. S3). Similar to other researchers'

findings, salts tended to negatively affect the formation of coacervates, due to their interference on the electrostatic interactions as well as on the electrostatic charge balance (Anema & de Kruif, 2014; Blocher McTigue & Perry, 2020). Considering the negative effect of salts on the SSP-LF coacervate formation, in our research design, salt was not included.

#### 3.2. Characterization of coacervate complex

### 3.2.1. Sodium dodecyl sulfate-polyacrylamide gel electrophoresis (SDS-PAGE)

To further understand if coacervate complexation influences the stoichiometry and the subunit of lactoferrin, SDS-PAGE of selective complex solutions that were obtained at their optimum conditions were analyzed (Fig. 4A). All the samples were diluted to the same protein concentration according to the ratio of SSP/LF in the mixtures. The SDS-PAGE showed that all the SSP-LF mixtures showed a similar profile with the native LF solutions, indicating that the coacervation did not change the polypeptide subunits of LF. LF exhibited a major molecular weight at around 75 kDa, which was consistent with the results reported by other researchers (Adal et al., 2017).

The obtained mixtures at each pH were further centrifuged to separate the polymer dense phase, the coacervates, and the polymer-poor phase, the supernatant. The gel-like coacervates after centrifugation and freeze-drying were shown in Fig. 4B. The yield of complex obtained at the optimal ratios at pH 4, 5, 6, and 7 was 33.7%, 51.1%, 12.7% and 6.7%, respectively. The supernatants were further diluted proportionally based on the SSP:LF ratio and then used for the SDS-PAGE analysis. The supernatant obtained at pH 5 showed the lightest polypeptide bands, especially the one at 75 kDa, indicating the least free LF present in this sample (Fig. 4A). The supernatant at pH 4 had slightly lighter polypeptide bands than the supernatants for pH 6 and pH 7, but darker bands than pH 5. The relative changes indicated different amounts of free LF. The lower amounts of free LF present in pH 5 and pH

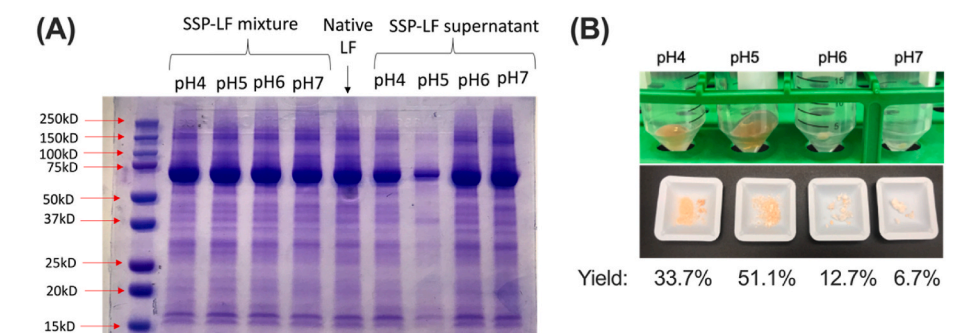


**Fig. 4.** (A) SDS-PAGE<sup>a</sup> of SSP-LF mixture and its supernatant obtained at optimal coacervate formation conditions. (B) optical images and yield of SSP-LF complex obtained after centrifugation and freeze-dry. Note:a For SDS-PAGE analysis, samples were diluted proportionally according to the ratio of LF in the mixture. (b) Optimal coacervate formation conditions refer to SSP-LF1:2 at pH 4, SSP-LF1:4 at pH 5, SSP-LF 1:8 at pH 6, and SSP-LF1:12 at pH 7.

4 supernatant confirmed that these two conditions favored complex coacervates formation with SSP. These results were consistent with the turbidity study that pH 5 showed the highest turbidity than pH 4, 6, and 7 at their corresponding optimal SSP:LF ratios, indicating the highest complexation.

#### 3.2.2. Structure of coacervate complex

Fourier-transform infrared spectroscopy (FTIR). The FTIR of freeze-dried complex samples was analyzed to investigate whether the formed complex affects any chemical bond changes of lactoferrin. The different bands present in the FTIR indicated the different functional groups in the biopolymer molecules (Fig. S4). Particularly, amides I-III are the most common regions referring to the confirmation and secondary structure of the protein. For native LF samples, the amide I, II, and III regions are located at 1637, 1514, and 1273 cm<sup>-1</sup>, respectively. The free amino acid O-H groups have been identified in the range of between 3170 and 3300 cm<sup>-1</sup>(Barth & Zscherp, 2002). The band at 1060 cm<sup>-1</sup> (around 1100 cm<sup>-1</sup>) was reported to relate to the stretching vibration of O-H and C-C bonds of sugar groups in protein (Lan et al., 2019). In SSP samples, the FTIR bands were similar to the ones reported in other polysaccharides. Specifically, the first (3291 cm<sup>-1</sup>), second  $(1609 \text{ cm}^{-1})$ , third  $(1438 \text{ cm}^{-1})$  and forth  $(1009 \text{ cm}^{-1})$  bands represent the O-H groups, carboxylic groups (-COO<sup>-</sup>), C-O bonds, and vibrational stretch of the C-O and C-C groups of SSP, respectively (Bastos et al., 2018).

The SSP-LF complex samples showed an FTIR result similar to the spectra of LF, consisting of bands at 3280, 1636, 1516, and 1273 cm<sup>-1</sup> that referred to the O-H group, amide I, II, and III, respectively. The region represented amide I group in LF showed a displacement of 1 cm in the region of  $1637~\text{cm}^{-1}$ , as a consequence of the electrostatic interaction between the -COO (C=O) group of SSP and the -NH<sup>3+</sup> (NH) group of LF, which was also observed by (Bastos et al., 2018). The right shift of bands (1060 cm<sup>-1</sup>) was reported to be related to sugar groups (1035-1055 cm<sup>-1</sup>) as a result of the glycosylation modification in complex samples (Lan et al., 2019). Some studies reported a shift of O-H groups of LF due to complexation with other protein or polysaccharides polymers due to hydrogen bonding (Zheng et al., 2020). Although this kind of shift was not observed in the current study probably because both biopolymers demonstrated an O-H peak at a similar region, the hydrogen bonding can easily occur between the hydroxyl groups of both biopolymers in the aqueous media.

Circular dichroism (CD) spectra. The CD of LF and SSP/LF solution samples were analyzed to investigate whether the coacervation complex affected the secondary structures of LF (Table S2 and Fig. S5). In our samples, LF had a positive peak at 196 nm and a negative peak at around 210 nm, indicating the  $\alpha/\beta$  structure of the LF protein. Our results indicated that our LF consisted of 16–20% of α-helix, 33–42% of β-strands, 10–12% of β-turns, and 30–34% of unordered structures (Table S2), this was similar to the results reported by other researchers (Sreedhara et al., 2010; Wang, Timilsena, et al., 2017). After forming a

complex with SSP, the CD spectra of LF in the SSP-LF mixture were similar to the one in LF solutions (Fig. S5-C&D). The  $\beta$ -strands content of LF in the complex seemed to be higher than individual LF however the change was not significant (Table S1). The retaining of protein secondary structure in the coacervate complex was also reported by other researchers (Zheng et al., 2021). Overall, the FTIR and CD spectra results indicate that no significant structural changes of LF was involved in the complex formation between SSP and LF.

#### 3.2.3. Microstructure analysis of coacervate complex

Scanning electron microscopy of LF, SSP, and SSP-LF complex were obtained at pH 5 and pH 7, as the representatives of insoluble and soluble complexes, respectively (Fig. 5). In vacuum-dried solution samples, the native LF (Fig. 5A) presented as tiny spherical particles even under a high magnitude (scale bar = 500 nm). However, SSP (Fig. 5B) displayed flake-like particles showing a larger size. These results were consistent with the particle size analysis of LF and SSP solutions, which displayed sizes of 60-70 nm and 200-300 nm, respectively. For the SSP-LF insoluble complex (formed at pH 5) (Fig. 5C), the particles were in spherical shapes with a size around 200-300 nm, demonstrating a completely different morphology from SSP and LF solutions. Therefore, these particles were the formed insoluble SSP/LF complex, rather than SSP or LF particles. For the SSP-LF soluble complex (formed at pH7) (Fig. 5D), the particles were as small as less than 100 nm, consistent with the particle size analysis results. The large SSP particles disappeared in this sample probably due to their low amount (the mass ratio of SSP/LF was 1:12) in the complex solutions so that SSP could be fully dispersed in the liquid

Different from the overnight vacuum-dried samples, the freeze-dried samples (Fig. 5E–H) showed clusters of particles due to the freeze-drying process. In LF samples, the spherical particles were connected in a line and further twisted in 3D structures (Fig. 5E). SSP were clustered into large flakes (Fig. 5F) as a consequence of the freeze-drying process. Compared to LF, SSP-LF (Fig. 5G) coacervate complex was clustered into even much larger spherical particles, due to its larger original sizes (Fig. 5C) than LF (Fig. 5A). Interestingly, the freeze-dried soluble complex (Fig. 5H) also presented as large spherical particles similar to the insoluble complex with SSP sheets, probably as a consequence of the freeze-drying process. In summary, the SEM analysis showed that insoluble SSP-LF coacervate formed at pH 5 had spherical-shape particles sizing around 200-300 nm while soluble SSP-LF complex formed at pH 7 were nano-sized particles with sizes less than 100 nm. The drying process also affects the morphology and complex sizes of the complex. The size and shape of vacuum-dried complex would be closer to the complex in solution samples, while the freeze-dried complex presents as clusters of particles in a larger size.

#### 3.3. Real time interaction between SSP and LF measured by QCM-D

To elucidate the interactions between SSP and LF, real-time Quartz

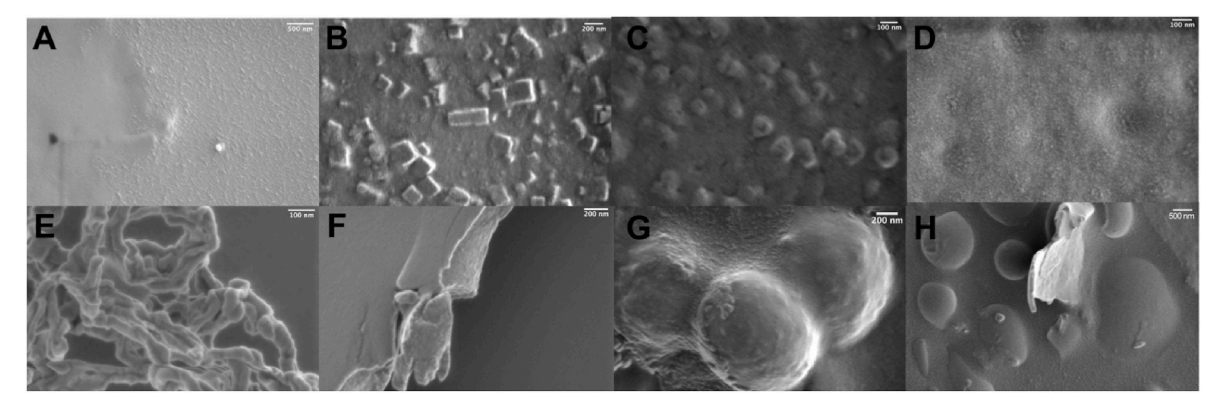


Fig. 5. SEM micrographs of LF, SSP, insoluble SSP-LF complex (pH 5), and soluble SSP-LF complex (pH 7) in the form of vacuum-dried solution samples (A–D) and freeze-dried samples (E–H).

Crystal Microbalance with Dissipation (QCM-D) technology was utilized in this study. The QCM-D frequency shifts with respect to time at different experimental stages were recorded to understand the interactions of LF and SSP (Fig. 6A). According to the changes in the frequency and the properties of added solution at each stage, the mass of solutions added on the surface of the sensor can be calculated (Fig. 6B). A separate experiment by feeding 1% SSP first to the system instead of LF followed by a rinsing step was performed (Fig. S6). The results showed that the frequency went back to the baseline level after rinsing the SSP layers, indicating the interactions between SSP and sensor were weak thus all SSP molecularly that directly attached to the sensor would be removed after the rinsing step. Accordingly, the mass increases after the last step of each QCM-D experiment (Fig. 6A) were solely from the SSP-LF layer. Depending on each set of experiments, the equilibrium time may be varied (Fig. 6A 1–4).

By comparing the amount of frequency drop after adding LF at different pH, it showed that the larger the pH, the larger drop of frequency (Fig. 6A 1-4). It was more evident after the water rinsing step that the frequency shift was about 30, 40, 70, and 80Hz at pH 4, 5, 6, and 7 (Fig. 6A 1-4). At the same time, the mass of the LF layer was increased along with the increase of pH (Fig. 6B), indicating an increased absorption of LF on the gold sensor. The result was consistent with previous studies that the absorption of protein surfaces was pH-dependent and it was higher when close to its pI (Bokkhim et al., 2013; Li et al., 2021; Teo et al., 2016). An increase of frequency drop when feeding with LF solutions in a higher pH condition was also observed by other researchers (Teo et al., 2016). The hydrophobicity of LF was increased along with the increase of pH when approaching its pI (8.0-9.0) due to the diminishing of ionized groups, thus the hydrophobic interactions between LF and sensor surface were enhanced, resulting in an increased drop of frequency.

After feeding the LF-coated sensor with SSP, the frequency drop was larger at pH 4/pH 5 than pH 6/pH 7 (Fig. 6A 1-4), mainly due to the stronger interactions between SSP and LF at the former conditions. After rinsing with water, loosely attached SSP molecules were removed, and the SSP-LF double-layer stayed on the surface. As shown in Fig. 6A, the final absolute value of frequency, related to the total mass of SSP-LF bilayers, was also increased along with the increase in pH, which was similar to the trend of the mass of the LF layer (Fig. 6B). The mass of the SSP layer on the sensor can be calculated by subtracting the mass of the LF layer by the mass of the SSP-LF double layers. Interestingly, the amount of SSP being adsorbed on the LF layers was highest at pH 5. One would expect to see the highest mass of the SSP layer at pH 4 considering that at pH 4, the zeta-potential of SSP is lower than pH 5 so that more SSP would be needed to compensate for the positive charge of LF. However, since the amount of LF absorbed on the gold sensor was larger at pH 5 than pH 4, therefore, more SSP molecules can interact with LF and stay on the sensor, thus a higher amount of SSP was retained at pH 5.

This result also indicated a strong interaction between SSP and LF at pH 5, which agrees with the previous section that the highest turbidity and strongest interactions were observed at pH 5 conditions. Although the amount of LF stayed on the gold sensor was higher in pH 6 and pH 7, the absorbed SSP was less, further indicating a weak interaction between SSP and LF. Because there was a lower charge density of LF in these pH conditions, less SSP was enough to interact with the charged patches in LF molecules. In total, the QCM-D results supported the hypothesis that the electrostatic interactions between SSP and LF play a critical role in formulating the SSP-LF complex. The formed complex may help to protect LF from thermal degradation, which will be comprehensively discussed in the following section. Additionally, the polysaccharidesprotein complex has been commonly used as an ingredient to stabilize emulsions and nano-emulsions. The current studies suggested that QCM-D can be an ideal tool to play as a simplified model of emulsion interface to investigate the interfacial structures of biopolymer on the hydrophobic surface under different pH conditions (Cao et al., 2021; Li et al., 2021; Teo et al., 2016, p. 201).

## 3.4. Effect of coacervate complexation on the thermal stability of lactoferrin

3.4.1. Turbidity and CD spectra of mixture samples after thermal treatment After obtaining and characterizing the SSP-LF coacervate complex and their interactions, the third goal of this study is to investigate whether the formed complex improved the thermal stability and antibacterial capacity of LF. Optical images and turbidity measurements of LF and SSP-LF mixtures prepared at pH 5 and pH 7 (as representatives of insoluble and soluble complex, as well as acidic and neutral conditions, respectively) at their optimal complex formation ratios (1:4 and 1:12, respectively) before and after thermal treatment (75 °C/85 °C/95 °C for 2 min) were collected (Fig. 7).

At pH 5, the native LF showed clear solutions before and after thermal treatment (Fig. 7A), with neglectable (p>0.05) changes in turbidity (Fig. 7E), indicating that the native LF was thermally stable under acidic conditions. However, native LF solutions at pH 7 become cloudier with increased turbidity due to the thermal aggregation of the protein (Fig. 7B). The relatively high thermal stability of LF at acidic conditions and low stability at neutral pH were also reported previously. Solutions of native LF have been reported to remain clear while heating at 90 °C for 5 min at acidic pH levels, they become turbid at neutral pH, and formed gels at alkaline pH levels (Abe et al., 1991). This is attributed to LF becoming less charged and thus more hydrophobic at neutral pH as it approaches the pI of LF. The increase in temperature enhances the hydrophobic bonds by weakening the hydrogen bonds, with the increase of surface hydrophobicity, causing protein aggregation and the increase of turbidity (Goulding et al., 2021; Mata et al., 1998).

After forming the complex with SSP, the initial SSP-LF samples at pH

Food Hydrocolloids 131 (2022) 107736

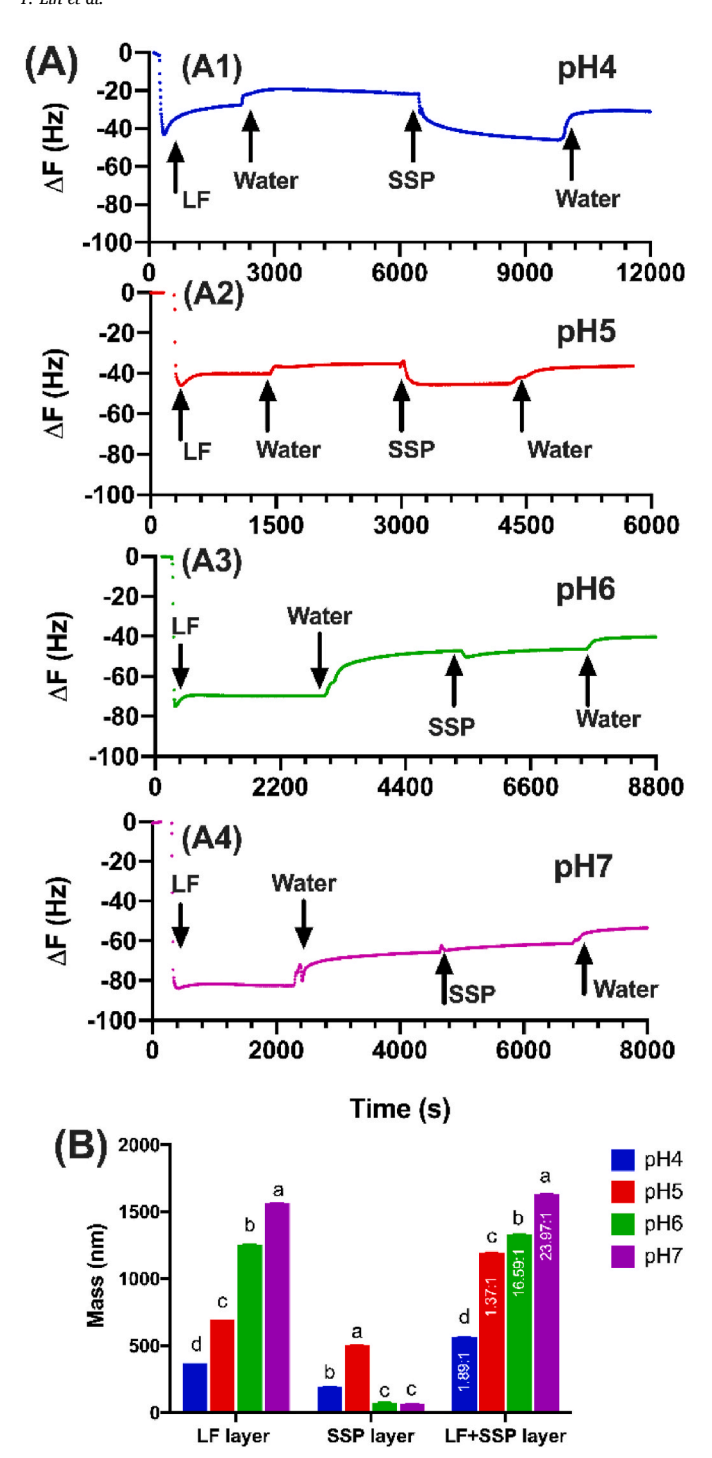


**Fig. 6.** (A) Frequency shift at 7th overtone and (B) the biopolymer layer thickness for the sequential adsorption of LF (first) and SSP solutions at the same pH (4, 5, 6 and 7) on the quartz crystal surface.

5 were cloudy since the complex was insoluble (Fig. 7C) while the samples at pH 7 were clear as they formed soluble complexes (Fig. 7D). After thermal treatment, SSP-LF samples at pH 5 showed neglectable (p >0.05) changes of appearance and turbidity (Fig. 7C and E). Although the turbidity of SSP-LF samples at pH 7 increased after thermal treatment, the increase was less than native LF samples at pH 7 (Fig. 7D&E). These results suggest that SSP-LF complex was thermally stable at acidic conditions (similar to native LF), and the SSP-LF soluble complex can help to reduce the thermal aggregation of LF at neutral pH.

CD spectra of native LF solutions and SSP-LF complex solutions

before and after thermal treatment were collected to understand the impact of heat on the secondary protein structures (Fig. 7A-D and Table S2). At pH 5, the CD spectra of both native LF and SSP-LF mixture showed an insignificant decrease of peak intensity at 190 nm and 210 nm before and after thermal treatment (Fig. 7A&C and Table S2) which is consistent with the turbidity results that both LF and SSP-LF were thermal stable at acidic conditions. At pH 7, native LF (Fig. 7C) showed a decrease of peak intensity at 190 nm and 210 nm after thermal treatment, resulting in a significant reduction of  $\alpha$ -helix (from 17% to 7%) and an increase of  $\beta$ -strands (from 37% to 51%) in LF samples (Table S2). Particularly, a perceptible loss of  $\alpha$ -helix occurred after thermal treatment at 75 °C/2min, and the loss of  $\alpha$ -helix was evident when the heating temperature was higher than 85 °C. Such changes indicated the loss of LF native structures and the alternation or redistribution of intra- or inter-molecular interactions. The decrease of the peak intensity of LF after thermal treatment was also reported previously, and their results were similar to what was observed in the current study (Goulding et al., 2021). The SSP-LF mixture at pH 7 showed an insignificant decrease of  $\alpha$ -helix (from 20% to 17%) and a significant increase of  $\beta$ -strands (from 39% to 46%) (Fig. 7D and Table S2). The secondary structure changes of SSP-LF mixtures at pH 7 were much less compared to pure LF solutions, indicating a higher structural stability than individual LF solutions during thermal treatment.

## 3.4.2. Turbidity and CD spectra of freeze-dried samples re-dispersed in solution after thermal treatment

Currently, interest in LF in the food industry has focused on dairy-derived food products such as infant formulas and milk-based beverages, the pH of these products is generally close to neutral. Therefore, another set of experiments was conducted to particularly focus on the pH 7 conditions (Fig. 8B). The freeze-dried SSP-LF complex samples obtained at pH 5 (the ratio of 1:4) were chosen as it showed the highest complex formation according to the turbidity study. The dried sample was redissolved in water and the pH was adjusted to pH 7 to mimic the procedures for the application of SSP-LF complex powder as an ingredient in milk delivered products. In addition, native LF solution (Fig. 8A) at the same mass ratio and the soluble complex of SSP and LF (Fig. 8B) directly prepared at the ratio 1:4 at pH 7 were used as a comparison.

After redispersion and pH adjustment, the freeze-dried samples were presented as clear solutions with a higher solubility (Fig. 8C), compared to the direct mixture sample at pH 5 (Fig. 7C). Due to the pH adjustment to 7, the structures of SSP-LF complex particles can be loosened and become soluble because of reduced electrostatic interactions between SSP and LF (da S. Gulão et al., 2014). After thermal treatment, native LF solutions showed the highest increase in cloudiness as well as the turbidity value (Fig. 8A and D). For both the SSP-LF mixtures and redissolved solutions (from freeze-dried samples), the increase in turbidity after heating was less than the native LF samples (Fig. 8D).

The CD spectra of native LF samples, and the SSP-LF mixtures (pH 7 1:4), and rehydrated SSP-LF pH 5 coacervate samples (adjust to pH 7) were also measured (Fig. 8A-D). The decrease of peak intensity for SSP-LF solutions (Fig. 8B) was less than LF (Fig. 8A). LF samples showed a significant decrease of  $\alpha$ -helix and increase of  $\beta$ -strands when the thermal treatment was higher than 85 °C, while the changes of secondary structures of SSP-LF solutions was only significant after being heated at 95 °C (Table S3). For the rehydrated SSP-LF samples (Fig. 8C), the decrease of peak intensity was lower and the change in secondary structures was insignificant during all the thermal treatments, indicating the highest retention of the structural integrity of LF (Table S3). The results indicated that both the freeze-dried samples and the soluble complex (at pH 7) can improve the thermal stability of LF at neutral conditions. Freeze dried samples showed even superior protection on LF as a consequence strengthened complex structures under freeze drying process.

Previous studies have reported that the presence of certain polysaccharides can improve the thermal stability of proteins without

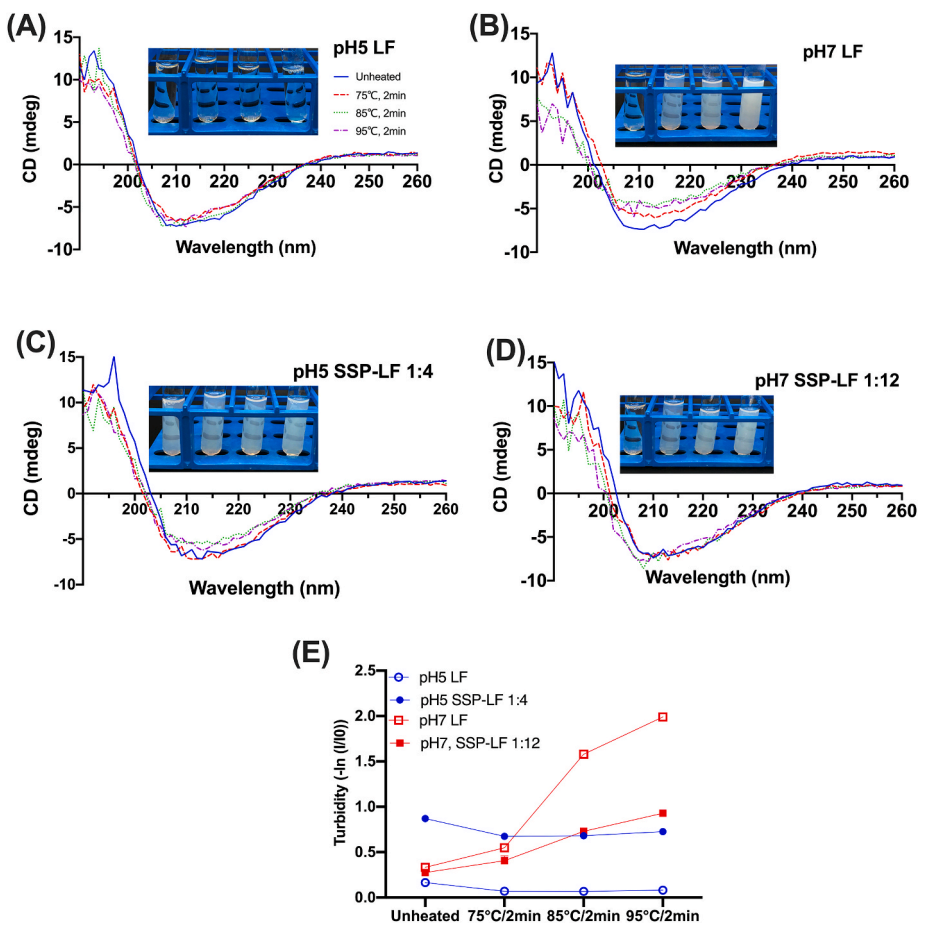


Fig. 7. (A–D) Optical images, CD spectra, and (E) turbidity of LF and SSP-LF mixtures prepared at pH 5 and pH 7 before and after thermal treatment (75 °C/85 °C/95 °C for 2min).

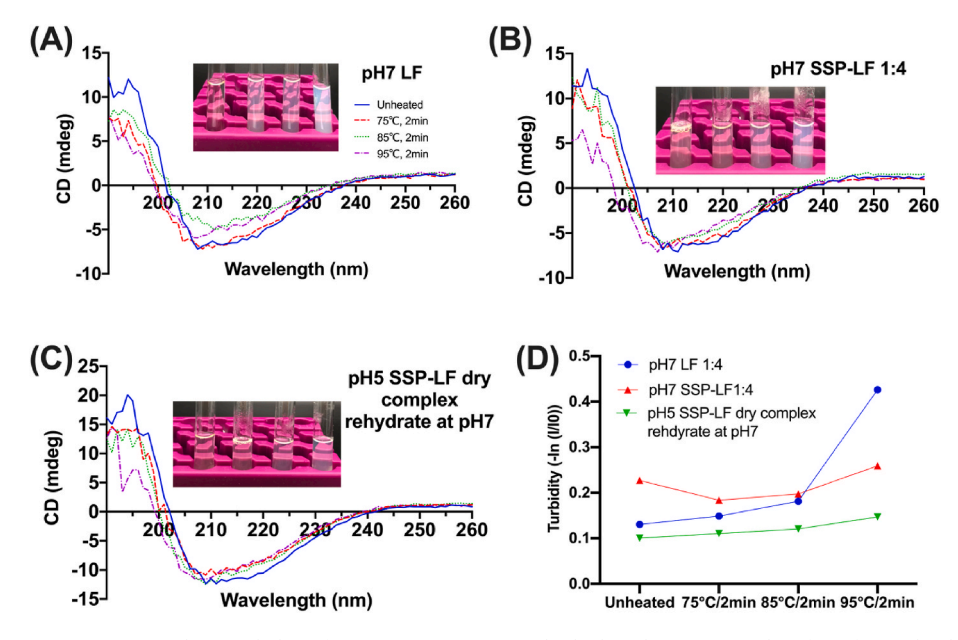


Fig. 8. (A–C) Optical images, CD spectra, and (D) turbidity of LF, SSP-LF mixtures, and rehydrated SSP-LF complex (from freeze dried samples) before and after thermal treatment (75  $^{\circ}$ C/85  $^{\circ}$ C/95  $^{\circ}$ C for 2min) at pH 7.

inducing any confirmation or aggregation at high temperatures (Bengoechea et al., 2011; Jones & McClements, 2010). For example, no significant changes in turbidity were presented in complex coacervates

containing 0.1% LF and 0.1% gum Arabic at pH 7 when heated from 25  $^{\circ}$ C to 90  $^{\circ}$ C (da S. Gulão et al., 2014). In the current study, both turbidity and CD spectra measurement results confirmed the prevention

of LF aggregation and change of its secondary structures upon forming coacervates complex with SSP. Upon heating, globular protein tends to unfold and expose the hydrophobic groups to the surrounding aqueous phase, which further leads to protein self-association and aggregation. The formed SSP-LF complex may help to reduce the exposure of the hydrophobic groups of LF thus reducing its aggregation during thermal treatment. Conversely, studies are finding that the impact of WPI and pectin (coacervate complex) on the thermal stability of WPI was pH-dependent (Gentès et al., 2010). These results showed that sample solutions (WPI/pectin) only remained stable at pH 4.5 after being heated at 76 °C, while at pH 7 protein denaturation was observed due to the loss of electrostatic attraction between WPI and pectin at neutral conditions. The different results among these studies suggested that the stability of the protein through complexation with biopolymers is dependent on the type of biopolymers and the given mixing and process conditions.

#### 3.4.3. DSC measurement

DSC thermograms of LF and SSP-LF complex samples (at pH 5-7) provide the thermal characteristics such as T<sub>p</sub> (peak temperature) and  $\Delta H$  (enthalpy change) of samples (Fig. S7 and Table S4). Due to the low amounts of samples that can be measured by the instrument and the low mass ratio of LF in the SSP-LF complex at pH 4 (SSP-LF, 1:2), the thermal behavior of these samples is too hard to observe thus are not shown. The DSC graph of LF showed two denaturation peaks (Fig. S7); The first peak appeared around 62  $^{\circ}$ C ( $T_p$ ) and the second one at 88  $^{\circ}$ C (Table S4). The enthalpy change of the first peak (-3.94 J/g) was larger than the second peak (-0.82 J/g) (Table S4), which corresponded to the N and C lobes of dumbbell-shaped LF. The different degrees of iron saturation and structural compactness of these two lobes are likely responsible for their different thermal behaviors. The first low thermal denaturation temperature at 60 °C also explained the low thermal stability of LF in our thermal treatment study as well as during food processing. The thermal denaturation peaks of lactoferrin were reported to be 76  $^{\circ}\text{C}$  and 95  $^{\circ}\text{C}$ (Zheng et al., 2020), while they were around 58 °C and 89 °C reported by other studies (Goulding et al., 2021). These variations in peak temperatures could come from the different iron saturation and structures of LF due to the protein sources and production procedures in the industry.

The complexation with SSP increased the onset and peak temperature of LF (Fig. S7 and Table S4). The improvement of denaturation

temperature of protein via complexation of polysaccharides has also been reported previously (Bengoechea et al., 2011; Bokkhim et al., 2015). Interestingly, the SSP-LF complex formed at pH 6 and 7 showed a higher denaturation temperature than the complex formed at pH 5, which can also be due to the higher iron saturation of LF at higher pH. LF is known to lose iron at lower pH and the iron saturation of LF can influence the thermal stability of LF as mentioned in the introduction (Wang et al., 2019). Nevertheless, the SSP-LF complex formed at pH 5 showed a higher denaturation temperature than native LF in a similar pH condition, which further demonstrated the interactions between SSP and LF could improve the thermal stability of LF.

### 3.5. Effect of coacervate complexation on the antimicrobial capacity of lactoferrin

The antimicrobial activity of LF and SSP-LF complexes before and after thermal treatment (Fig. 9) were measured to investigate whether the complexed LF remained functionally active and whether the activity can be retained after thermal treatment. The freeze-dried complex formed at pH 5 was used to compare with LF, as this complex showed the highest yield and the highest thermal stability with lowest structural changes among the formed complexes in the current study. The Staphylococcus aureus was chosen as the target bacteria as it is a common pathogenic bacterium that exists in dairy products. After 24h of incubation, both LF and SSP-LF significantly reduced the growth of Staphylococcus aureus compared with the control groups (medium only), while SSP solutions have no antibacterial effect. It is likely that the SSP is being used as an energy source by the bacteria as these solutions promoted the growth of Staphylococcus aureus compared with the control group. This observation means that the antibacterial capacity of the SSP-LF complex was solely from LF, rather than SSP. These results also indicate that the complexation of LF with SSP maintains the antibacterial activity of LF. After being thermally treated at 75 °C/2 min, heated LF showed an increase in bacterial growth, reaching an amount close to the control group indicating that thermal treatment significantly impedes the antibacterial capacity of LF. Heated SSP still showed a similar promotional effect with unheated SSP on the growth of bacteria, which can be expected since the heating would not influence SSP's ability to be utilized by the bacteria as a feedstock. Heated SSP-LF samples, however, showed

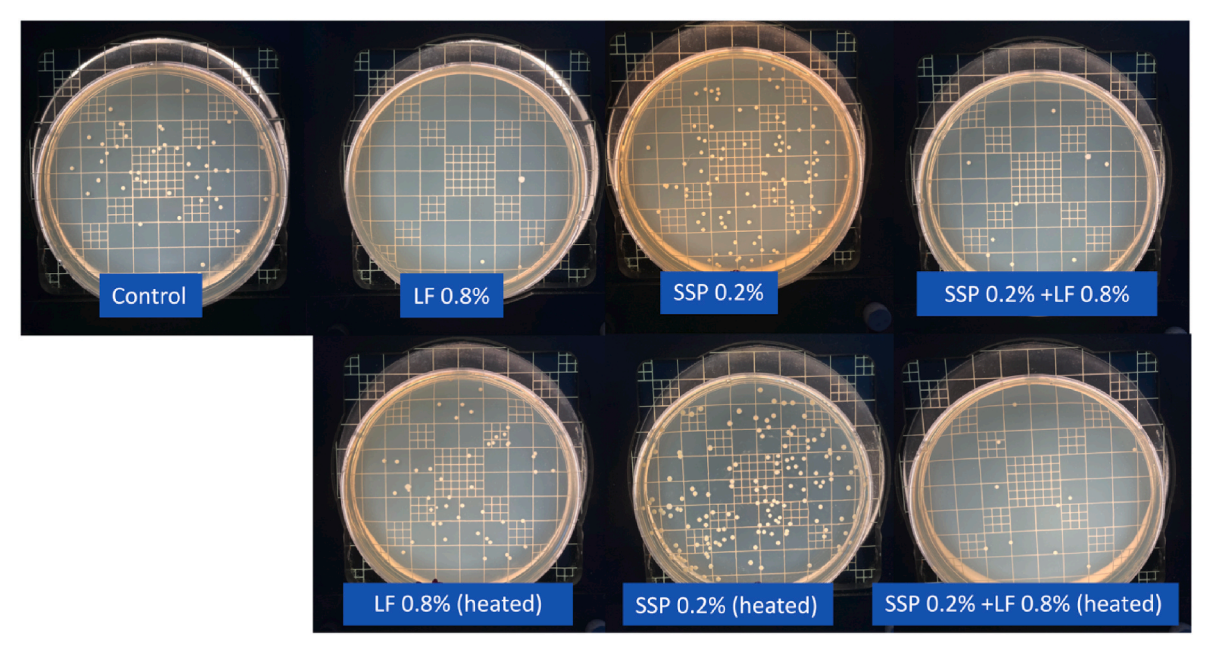


Fig. 9. Antimicrobial effect of LF and SSP-LF complex before and after thermal treatment at 75 °C/2min against the growth of 10<sup>6</sup> diluted *Staphylococcus aureus* after 24 h of incubation.

a similar inhibitory effect on bacterial growth as unheated SSP-LF samples, providing evidence that the SSP-LF complex retains the antibacterial activity of LF even after thermal treatment. The protection of LF anti-bacterial activity could be attributed to the retention of the LF structure in SSP-LF complex, as evidenced by the turbidity and CD studies. Overall, these results demonstrated that the complexation of LF with SSP did not affect the antibacterial activity of LF even under thermal processing conditions.

#### 4. Conclusions

This study demonstrated that soy soluble polysaccharides, as soybean byproducts, have the potential to be utilized as sustainable materials to form a complex with LF to improve the thermal stability as well as the functionality, such as antibacterial activity, of LF. Both insoluble and soluble SSP-LF complexes could be formulated depending on the SSP/LF ratio and pH conditions. As observed by the SEM, the insoluble SSP-LF complex were sphere particles with a diameter of 200-300 nm, while the soluble SSP-LF complex was presented as poriferous particles with much smaller particle size. Their different structures and sizes can result from the strength of the electrostatic interactions between SSP and LF. The real-time interactions between SSP and LF were successfully evaluated and quantified through QCM-D at a hydrophobic surface. The freeze dried SSP-LF complex formed at pH 5 (then redispersed in neutral pH) provided more protection on the thermal stability of LF compared to the complex directly formed at pH 7, mainly due to the drying process and stronger interaction between SSP and LF at pH 5. The improved stability further promoted the SSP-LF complex to retain the antimicrobial capacity of LF during thermal treatment. Nevertheless, whether other negatively charged biopolymers including polysaccharides and proteins have the potential to improve the thermal stability of the LF by complex coacervation still needs further exploration. Particularly it would be interesting to study dairy by-products such as whey protein isolates or hydrolysates, considering commercial LF is mainly extracted from bovine milk (Lin et al., 2021). Furthermore, since the modification of higher order (secondary, tertiary and quaternary) structures would impact the functional properties of LF, it is worthy to investigate, in detail, the relationship between LF confirmational changes and its functionality.

#### Author contributions

**Tiantian Lin:** Conceptualization, data curation, formal analysis, investigation, methodology, writing-original draft, writing-review & editing.

Younas Dadmohammadi: Conceptualization, project administration, writing-review & editing.

**Seyed Mohammad Davachi**: Investigation, writing-review & editing.

Hooman Torabi: Investigation, writing-review & editing.

Peilong Li: Investigation, writing-review & editing.

Benjamin Pomon: Investigation, writing-review & editing.

Gopinathan Meletharayil: Resources, writing-review & editing.

Rohit Kapoor: Resources, writing-review & editing.

**Alireza Abbaspourrad:** Funding acquisition, resources, supervision, writing-review & editing.

#### Declaration of competing interest

All the authors declare no conflict of interest.

#### Acknowledgments

The authors acknowledge the funding support from the National Dairy Council (Rosemont, IL). The authors would like to thank Nanoscience Instruments and Biolin Scientific for providing the QCM-D equipment, the QSense Analyzer, and for their generous technical support. The authors would also like to thank Dr. Crane for the use of CD spectroscopy and Rebecca Zawistowski for her technical support. This work made use of the SEM facility from the Cornell Center for Materials Research (CCMR) supported by the National Science Foundation under Award Number DMR-1719875. This work also made use of the DSC facility from the Cornell Energy Systems Institute (CESI).

#### Appendix A. Supplementary data

Supplementary data to this article can be found online at https://doi.org/10.1016/j.foodhyd.2022.107736.

#### References

- Abe, H., Saito, H., Miyakawa, H., Tamura, Y., Shimamura, S., Nagao, E., & Tomita, M. (1991). Heat stability of bovine lactoferrin at acidic pH. *Journal of Dairy Science*, 74 (1), 65–71. https://doi.org/10.3168/jds.S0022-0302(91)78144-7
- Adal, E., Sadeghpour, A., Connell, S., Rappolt, M., Ibanoglu, E., & Sarkar, A. (2017). Heteroprotein complex formation of bovine lactoferrin and pea protein isolate: A multiscale structural analysis. *Biomacromolecules*, 18(2), 625–635. https://doi.org/ 10.1021/acs.biomac.6b01857
- Anema, S. G., de Kruif, C. G., & Kees). (2014). Complex coacervates of lactotransferrin and β-lactoglobulin. *Journal of Colloid and Interface Science*, 430, 214–220. https://doi.org/10.1016/j.jcis.2014.05.036
- Barth, A., & Zscherp, C. (2002). What vibrations tell us about proteins. Quarterly Reviews of Biophysics, 35(4), 369–430. https://doi.org/10.1017/s0033583502003815
- Bastos, L. P. H., de Carvalho, C. W. P., & Garcia-Rojas, E. E. (2018). Formation and characterization of the complex coacervates obtained between lactoferrin and sodium alginate. *International Journal of Biological Macromolecules*, 120, 332–338. https://doi.org/10.1016/j.ijbiomac.2018.08.050
- Bengoechea, C., Jones, O. G., Guerrero, A., & McClements, D. J. (2011). Formation and characterization of lactoferrin/pectin electrostatic complexes: Impact of composition, pH and thermal treatment. Food Hydrocolloids, 25(5), 1227–1232. https://doi.org/10.1016/j.foodhyd.2010.11.010
- Blocher McTigue, W. C., & Perry, S. L. (2020). Protein encapsulation using complex coacervates: What nature has to teach us. Small, 16(27), Article 1907671. https:// doi.org/10.1002/smll.201907671
- Bokkhim, H., Bansal, N., Grøndahl, L., & Bhandari, B. (2013). Physico-chemical properties of different forms of bovine lactoferrin. Food Chemistry, 141(3), 3007–3013. https://doi.org/10.1016/j.foodchem.2013.05.139
- Bokkhim, H., Bansal, N., Grøndahl, L., & Bhandari, B. (2015). Interactions between different forms of bovine lactoferrin and sodium alginate affect the properties of their mixtures. Food Hydrocolloids, 48, 38–46. https://doi.org/10.1016/j. foodbyd/2014.12.036
- Brisson, G., Britten, M., & Pouliot, Y. (2007). Heat-induced aggregation of bovine lactoferrin at neutral pH: Effect of iron saturation. *International Dairy Journal*, 17(6), 617–624. https://doi.org/10.1016/j.idairyj.2006.09.002
- Campione, E., Lanna, C., Cosio, T., Rosa, L., Conte, M. P., Iacovelli, F., Romeo, A., Falconi, M., Del Vecchio, C., Franchin, E., Lia, M. S., Minieri, M., Chiaramonte, C., Ciotti, M., Nuccetelli, M., Terrinoni, A., Iannuzzi, I., Coppeda, L., Magrini, A., & Bianchi, L. (2021). Lactoferrin against SARS-CoV-2: In vitro and in silico evidences. Frontiers in Pharmacology, 12, 1524. https://doi.org/10.3389/fphar.2021.666600
- Cao, Y.-Q., Huang, G.-Q., Li, X.-D., Guo, L.-P., & Xiao, J.-X. (2021). Complex coacervation of carboxymethyl konjac glucomannan and ovalbumin and coacervate characterization. *Journal of Dispersion Science and Technology*, 1–11. https://doi.org/ 10.1080/01932691.2021.1888747
- Conesa, C., Rota, C., Castillo, E., Pérez, M. D., Calvo, M., & Sánchez, L. (2010). Effect of heat treatment on the antibacterial activity of bovine lactoferrin against three foodborne pathogens. *International Journal of Dairy Technology*, 63(2), 209–215. https://doi.org/10.1111/j.1471-0307.2010.00567.x
- Gentès, M.-C., St-Gelais, D., & Turgeon, S. L. (2010). Stabilization of whey protein Isolate—Pectin complexes by heat. *Journal of Agricultural and Food Chemistry*, 58(11), 7051–7058. https://doi.org/10.1021/jf100957b
- Goulding, D. A., O'Regan, J., Bovetto, L., O'Brien, N. M., & O'Mahony, J. A. (2021). Influence of thermal processing on the physicochemical properties of bovine lactoferrin. *International Dairy Journal*, 105001. https://doi.org/10.1016/j. idairyi.2021.105001
- Jenssen, H., & Hancock, R. E. W. (2009). Antimicrobial properties of lactoferrin. Biochimie, 91(1), 19–29. https://doi.org/10.1016/j.biochi.2008.05.015
- Jones, O. G., & McClements, D. J. (2010). Functional biopolymer particles: Design, fabrication, and applications. Comprehensive Reviews in Food Science and Food Safety, 9(4), 374–397. https://doi.org/10.1111/j.1541-4337.2010.00118.x
- Kilic, E., Novoselova, M. V., Lim, S. H., Pyataev, N. A., Pinyaev, S. I., Kulikov, O. A., Sindeeva, O. A., Mayorova, O. A., Murney, R., Antipina, M. N., Haigh, B., Sukhorukov, G. B., & Kiryukhin, M. V. (2017). Formulation for oral delivery of lactoferrin based on bovine serum albumin and tannic acid multilayer microcapsules. Scientific Reports, 7(1), 44159. https://doi.org/10.1038/srep44159
- King, J. C. J., Cummings, G. E., Guo, N., Trivedi, L., Readmond, B. X., Keane, V., Feigelman, S., & Waard, R. de (2007). A double-blind, placebo-controlled, pilot study of bovine lactoferrin supplementation in bottle-fed infants. *Journal of Pediatric*

- Gastroenterology and Nutrition, 44(2), 245–251. https://doi.org/10.1097/01.
- de Kruif, C. G., Weinbreck, F., & de Vries, R. (2004). Complex coacervation of proteins and anionic polysaccharides. Current Opinion in Colloid & Interface Science, 9(5), 340–349. https://doi.org/10.1016/j.cocis.2004.09.006
- Lan, Q., Li, L., Dong, H., Wu, D., Chen, H., Lin, D., Qin, W., Yang, W., Vasanthan, T., & Zhang, Q. (2019). Effect of soybean soluble polysaccharide on the formation of Glucono-8-Lactone-induced soybean protein isolate gel. *Polymers*, 11(12). https://doi.org/10.3390/polym11121997
- Lin, T., Meletharayil, G., Kapoor, R., & Abbaspourrad, A. (2021). Bioactives in bovine milk: Chemistry, technology, and applications. *Nutrition Reviews*, 79(Supplement\_2), 48–69. https://doi.org/10.1093/nutrit/nuab099
- Li, H., Wu, J., Doost, A. S., Su, J., & Van der Meeren, P. (2021). Electrostatic interaction between whey proteins and low methoxy pectin studied by quartz crystal microbalance with dissipation monitoring. *Food Hydrocolloids*, 113, Article 106489. https://doi.org/10.1016/j.foodhyd.2020.106489
- Lönnerdal, B., & Iyer, S. (1995). Lactoferrin: Molecular structure and biological function. Annual Review of Nutrition, 15(1), 93–110. https://doi.org/10.1146/annurev. pu 15 020195 000521
- Mata, L., Sánchez, L., Headon, D. R., & Calvo, M. (1998). Thermal denaturation of human lactoferrin and its effect on the ability to bind iron. *Journal of Agricultural and Food Chemistry*, 46(10), 3964–3970. https://doi.org/10.1021/jf980266d
- Mirabelli, C., Wotring, J. W., Zhang, C. J., McCarty, S. M., Fursmidt, R., Pretto, C. D., Qiao, Y., Zhang, Y., Frum, T., Kadambi, N. S., Amin, A. T., O'Meara, T. R., Spence, J. R., Huang, J., Alysandratos, K. D., Kotton, D. N., Handelman, S. K., Wobus, C. E., Weatherwax, K. J., & Sexton, J. Z. (2021). Morphological cell profiling of SARS-CoV-2 infection identifies drug repurposing candidates for COVID-19. Proceedings of the National Academy of Sciences, 118(36). https://doi.org/10.1073/pnas.2105815118
- Moore, S. A., Anderson, B. F., Groom, C. R., Haridas, M., & Baker, E. N. (1997). Three-dimensional structure of diferric bovine lactoferrin at 2.8 A resolution. *Journal of Molecular Biology*, 274(2), 222–236. https://doi.org/10.1006/jmbi.1997.1386
- Nakamura, A., Furuta, H., Maeda, H., Nagamatsu, Y., & Yoshimoto, A. (2001). Analysis of structural components and molecular construction of soybean soluble polysaccharides by stepwise enzymatic degradation. Bioscience Biotechnology and Biochemistry, 65(10), 2249–2258. https://doi.org/10.1271/bbb.65.2249
- Nakamura, A., Takahashi, T., Yoshida, R., Maeda, H., & Corredig, M. (2004). Emulsifying properties of soybean soluble polysaccharide. Food Hydrocolloids, 18(5), 795–803. https://doi.org/10.1016/j.foodhyd.2003.12.005
- Niu, Z., Loveday, S. M., Barbe, V., Thielen, I., He, Y., & Singh, H. (2019). Protection of native lactoferrin under gastric conditions through complexation with pectin and chitosan. Food Hydrocolloids, 93, 120–130. https://doi.org/10.1016/j. foodhyd.2019.02.020
- Nojima, Y., Suzuki, Y., Iguchi, K., Shiga, T., Iwata, A., Fujimoto, T., Yoshida, K., Shimizu, H., Takeuchi, T., & Sato, A. (2008). Development of poly(ethylene glycol) conjugated lactoferrin for oral administration. *Bioconjugate Chemistry*, 19(11), 2253–2259. https://doi.org/10.1021/bc800258v
- da, S., Gulão, E., de Souza, C. J. F., da Silva, F. A. S., Coimbra, J. S. R., & Garcia-Rojas, E. E. (2014). Complex coacervates obtained from lactoferrin and gum Arabic: Formation and characterization. Food Research International, 65, 367–374. https://doi.org/10.1016/j.foodres.2014.08.024
- Sreedhara, A., Flengsrud, R., Langsrud, T., Kaul, P., Prakash, V., & Vegarud, G. E. (2010).
  Structural characteristic, pH and thermal stabilities of apo and holo forms of caprine and bovine lactoferrins. *Biometals*, 23(6), 1159–1170. https://doi.org/10.1007/s10534-010-9366-5

- Teo, A., Dimartino, S., Lee, S. J., Goh, K. K. T., Wen, J., Oey, I., Ko, S., & Kwak, H.-S. (2016). Interfacial structures of whey protein isolate (WPI) and lactoferrin on hydrophobic surfaces in a model system monitored by quartz crystal microbalance with dissipation (QCM-D) and their formation on nanoemulsions. Food Hydrocolloids, 56, 150–160. https://doi.org/10.1016/j.foodhyd.2015.12.002
- Ueno, H. M., Ueda, N., Morita, M., Kakehi, Y., & Kobayashi, T. (2012). Thermal stability of the iron–lactoferrin complex in aqueous solution is improved by soluble soybean polysaccharide. Food Biophysics, 7(3), 183–189. https://doi.org/10.1007/s11483-012-9256-1
- Vogel, H. J. (2012). Lactoferrin, a bird's eye view. Biochemistry and Cell Biology, 90(3), 233–244. https://doi.org/10.1139/o2012-016
- Wang, B., Blanch, E., Barrow, C. J., & Adhikari, B. (2017). Preparation and study of digestion behavior of lactoferrin-sodium alginate complex coacervates. *Journal of Functional Foods*, 37, 97–106. https://doi.org/10.1016/j.jff.2017.07.044
- Wang, B., Timilsena, Y. P., Blanch, E., & Adhikari, B. (2017). Mild thermal treatment and in-vitro digestion of three forms of bovine lactoferrin: Effects on functional properties. *International Dairy Journal*, 64, 22–30. https://doi.org/10.1016/j. idairyj.2016.09.001
- Wang, B., Timilsena, Y. P., Blanch, E., & Adhikari, B. (2019). Lactoferrin: Structure, function, denaturation and digestion. Critical Reviews in Food Science and Nutrition, 59(4), 580–596. https://doi.org/10.1080/10408398.2017.1381583
- Wotring, J. W., Fursmidt, R., Ward, L., & Sexton, J. Z. (2022). Evaluating the in vitro efficacy of bovine lactoferrin products against SARS-CoV-2 variants of concern. *Journal of Dairy Science*. https://doi.org/10.3168/jds.2021-21247. S0022030222001151.
- Yan, B., Davachi, S. M., Ravanfar, R., Dadmohammadi, Y., Deisenroth, T. W., Pho, T. V., Odorisio, P. A., Darji, R. H., & Abbaspourrad, A. (2021). Improvement of vitamin C stability in vitamin gummies by encapsulation in casein gel. Food Hydrocolloids, 113, Article 106414. https://doi.org/10.1016/j.foodhyd.2020.106414
- Yao, X., Bunt, C., Cornish, J., Quek, S.-Y., & Wen, J. (2015). Oral delivery of bovine lactoferrin using pectin- and chitosan-modified liposomes and solid Lipid particles: Improvement of stability of lactoferrin. *Chemical Biology & Drug Design*, 86(4), 466–475. https://doi.org/10.1111/cbdd.12509
- Zamani, H., Zamani, S., Zhang, Z., & Abbaspourrad, A. (2020). Exceptional colloidal stability of acidified whey protein beverages stabilized by soybean soluble polysaccharide. *Journal of Food Science*, 85(4), 989–997. https://doi.org/10.1111/ 1750-3841.15041
- Zhang, Z., Cho, S., Dadmohammadi, Y., Li, Y., & Abbaspourrad, A. (2021). Improvement of the storage stability of C-phycocyanin in beverages by high-pressure processing. *Food Hydrocolloids*, 110, Article 106055. https://doi.org/10.1016/j. foodhyd.2020.106055
- Zhang, D.-Y., Qi, J.-R., Jiang, W.-X., Liao, J.-S., & Yang, X.-Q. (2021). Extraction and characterisation of pectin polysaccharide from soybean dreg and its dispersion stability in acidified milk drink. *International Journal of Food Science and Technology*, 56(10), 5230–5241. https://doi.org/10.1111/jiifs.15263
- Zheng, J., Gao, Q., Ge, G., Wu, J., Tang, C., Zhao, M., & Sun, W. (2021). Heteroprotein complex coacervate based on β-conglycinin and Lysozyme: Dynamic protein exchange, thermodynamic mechanism, and Lysozyme activity. *Journal of Agricultural* and Food Chemistry, 69(28), 7948–7959. https://doi.org/10.1021/acs.jafc.1c02204
- Zheng, J., Gao, Q., Tang, C., Ge, G., Zhao, M., & Sun, W. (2020). Heteroprotein complex formation of soy protein isolate and lactoferrin: Thermodynamic formation mechanism and morphologic structure. *Food Hydrocolloids*, 100, Article 105415. https://doi.org/10.1016/j.foodhyd.2019.105415